

In-Situ Construction of Crystalline/Amorphous Interface in SnO₂/Bi Nanobelts for Efficient CO₂ Electroreduction

Hanjun Li,^a Guangtong Hai,^{*b} Zhenyu Wang,^c Xin Chen,^a Shuxing Bai,^d Nan Zhang,^{*a} and Tianxi Liu^{*a}

^aKey Laboratory of Synthetic and Biological Colloids, Ministry of Education, School of Chemical and Material Engineering, Jiangnan University, Wuxi, 214122, China.

^bInstitute of Zhejiang University-Quzhou, Zhejiang University, Quzhou, 324000, China.

^cInstitute of Environmental Processes and Pollution Control, School of Environment and Ecology, Jiangnan University, Wuxi, 214122, China.

^dCollege of Chemistry and Chemical Engineering, Qingdao University, Qingdao, 266071, China.

*Address correspondence to: haigt@zju.edu.cn (G. T. Hai), nzhang@jiangnan.edu.cn (N. Zhang), txliu@jiangnan.edu.cn (T. X. Liu)

EXPERIMENTAL SECTION

Chemicals. Polyvinyl pyrrolidone (PVP) ($M_w=130000$) was purchased from J&K China Chemical Ltd (Shanghai, China). Bismuth nitrate pentahydrate ($\text{Bi}(\text{NO}_3)_3 \cdot 5\text{H}_2\text{O}$), Stannous chloride dihydrate ($\text{SnCl}_2 \cdot 2\text{H}_2\text{O}$) were purchased from Shanghai Aladdin Biochemical Technology Co., Ltd. N,N-Dimethylformamide (DMF) was purchased from Sinopharm Chemical Reagent Co. Ltd (Shanghai, China). The deionized water (H_2O) ($18 \text{ M}\Omega \text{ cm}^{-1}$) used in all experiments was prepared by (or passing water through) an ultra-pure purification system (Aqua Solutions).

Characterizations. Scanning electron microscopy (SEM) images and energy-dispersive X-ray spectroscopy (EDS) were characterized with a HITACHI S-4800 at 20 kV. The samples were prepared by dropping ethanol dispersion of samples on carbon-coated copper transmission electron microscopy (TEM) grids using pipettes and dried under the ambient condition. Low-magnification TEM images were obtained on a HITACHI HT7700 transmission electron microscope with an applied

acceleration voltage of 120 kV. High-magnification TEM and scanning TEM (STEM) images were acquired on an FEI Tecnai F20 transmission electron microscope with an acceleration voltage of 200 kV. Powder X-ray diffraction (PXRD) patterns of the samples were measured on a D8 Advance instrument (AXS-Bruker) with Cu K α radiation. X-ray photoelectron spectroscopy (XPS) analysis was done with an Axis supra. The carbon peak at 284.6 eV was used as a reference to correct the charging effects. Agilent 600 MHz nuclear magnetic resonance (NMR) spectroscopy was used to identify and quantify the yield of products in liquid electrolytes. X-ray absorption spectroscopy (XAS) measurements were carried out at the BL14W1 station in Shanghai Synchrotron Radiation Facility (SSRF, 3.5 GeV, 250 mA in maximum, Si (311) double-crystals). Attenuated total reflection infrared absorption spectroscopy (ATR-IRAS) was performed using the Thermo Scientific Nicolet iS20. Inductively coupled plasma mass spectrometry (ICP-MS) was employed with a Triple Quadrupole ICAP TQ ICP-MS.

CO₂ electroreduction in H-Cell. A three-electrode system was used to perform the electrochemical CO₂ reduction in H cell. An L-type glassy-carbon electrode (5 mm, 0.196 cm²) was used as the working electrode. A micro Ag/AgCl electrode (4.0 M KCl) and a carbon rod were used as reference electrode and counter electrode, respectively. The catalyst ink was prepared by ultrasonication 5 mg of catalyst with 490 μ L of ethanol and 10 μ L of 5 wt % Nafion solutions for 1 h. A 20 μ L of suspension was then deposited on glass carbon to prepare the working electrodes. Electrochemical reduction of CO₂ was conducted in a gastight H-cell separated by a cation exchange membrane (Nafion 117) on a CHI660 (Chenhua, Shanghai) electrochemical workstation. Each chamber contained 10 mL of 0.1 M KHCO₃ aqueous solution. As for the electrochemical measurements, CO₂ was delivered into the cathodic compartment (directly connected to the gas chromatograph) at a constant rate of 20 sccm and was allowed to purge for 30 min before the beginning of experiments. Then, CO₂ Electroreduction (CO₂RR) was tested by the chronoamperometry method under different potentials. The gas phase composition was analyzed by a gas chromatography system which was equipped with a flame ionization detector (FID) and a thermal conductivity detector (TCD). Liquid products were

characterized by ^1H NMR on Agilent 600 MHz DirectDrive2 spectrometers. ^1H chemical shifts were referenced to residual protic solvent signals. All potentials were calibrated to the reversible hydrogen electrode (RHE) reference. The Faradaic efficiency (FE) for the formation of reduction products was calculated as follows: $\text{FE} = eF \times n/Q = eF \times n/(I \times t)$, where e is the number of electrons transferred, F is the Faraday constant, Q is the charge, I is the current, t is the running time, and n is the total amount of product (in moles).

CO₂ electroreduction in flow-cell. The CO₂RR measurement in flow-cell was studied at room temperature under ambient pressure using a three-electrode setup in a flow-cell reactor with an Autolab PGSTAT302N potentiostat. The prepared catalyst was used as work electrode, the work electrode reaction area was 0.5 cm², while the catalysts were sprayed on a carbon paper substrate with the mass loading of 6 mg cm⁻² for CO₂RR. Ni foam was used as the counter electrode in 1 M KOH (pH=13.5). CO₂ was passed through the cathodic compartment at a constant flow rate of 30 sccm.

Density-functional theory (DFT). All the DFT computations were performed using the Cambridge Sequential Total Energy Package (CASTEP)^[1] based on the pseudopotential plane wave (PPW) method. Electron-ion interactions were described using the ultrasoft (USP) potentials^[2]. A plane-wave basis set was employed to expand the wave functions with a cutoff kinetic energy of 400 eV. For the electron-electron exchange and correlation interactions, the functional parametrized by Perdew-Burke-Ernzerhof (PBE)^[3], a form of the general gradient approximation (GGA), was used throughout. The vander Waals interaction was described using the DFT-D2 method that proposed by Grimme^[4].

During the geometry optimizations, all the atom positions were allowed to relax. In this work, the Brillouin-zone integrations were conducted using Monkhorst-Pack (MP) grids^[5] of special points with the separation of 0.05 Å⁻¹ for the model cell. The convergence criterion for the electronic self-consistent field (SCF) loop was set to 1×10⁻⁶ eV/atom. The atomic structures were optimized until the residual forces were below 0.03 eVÅ⁻¹.

Supplementary Figures and Tables

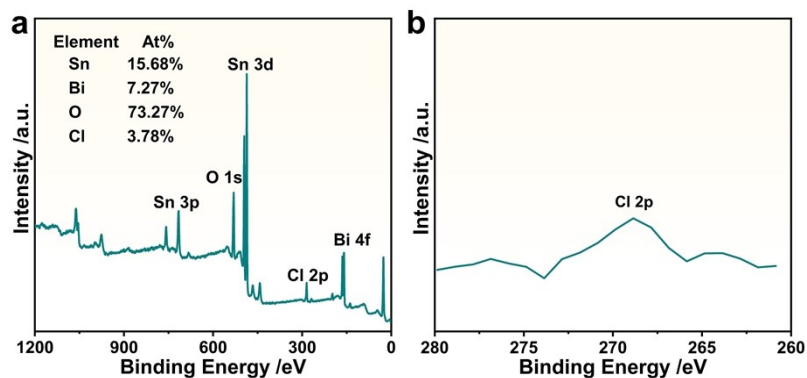


Fig. S1. (a) XPS survey spectrum, (b) the magnification of Cl 2p peaks for crystalline/amorphous (C/A)-SnO₂/BiOCl.

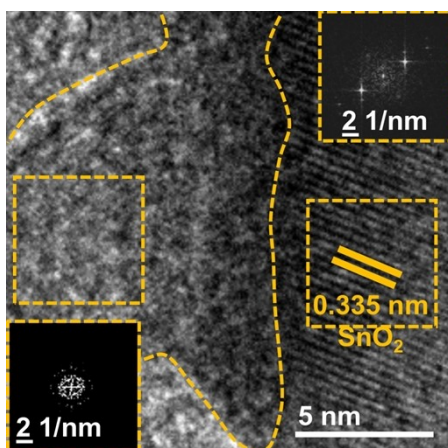


Fig. S2. HRTEM image of C/A-SnO₂/Bi (insert: corresponding fast Fourier transform images).

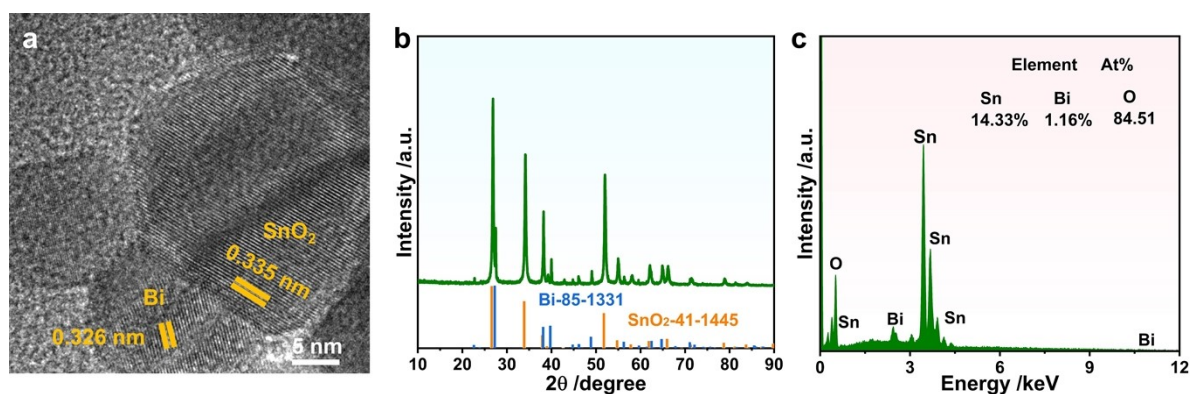


Fig. S3. (a) HRTEM image, (b) PXRD pattern and (c) SEM-EDS spectrum of crystalline/crystalline (C/C)-SnO₂/Bi.

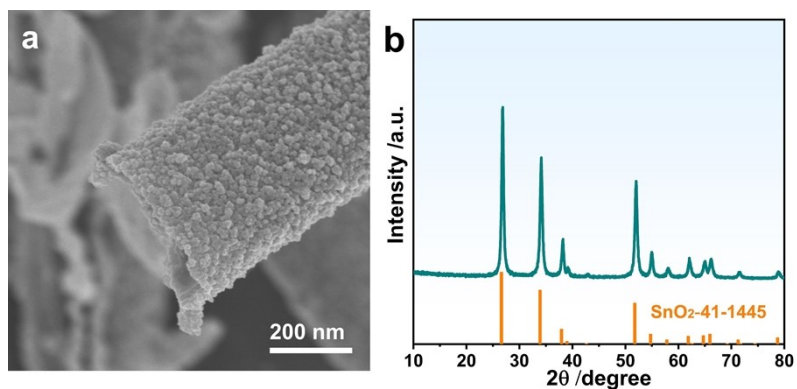


Fig. S4. (a) SEM image and (b) PXRD pattern of SnO₂.

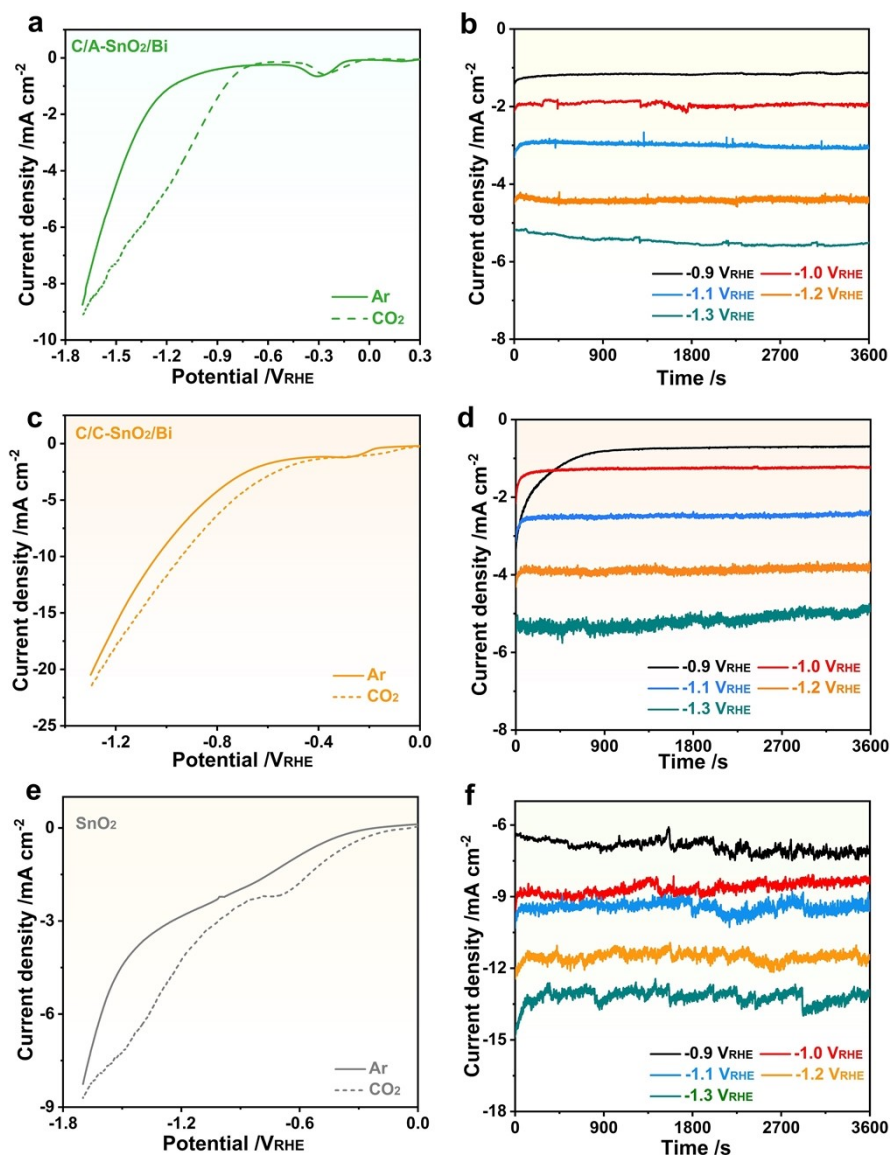


Fig. S5. LSV curves in the presence in Ar- or CO₂-saturated 0.1 M KHCO₃ aqueous solution of the (a) C/A-SnO₂/Bi and (c) C/C-SnO₂/Bi and (e) SnO₂ and chronoamperometry results of (b) C/A-SnO₂/Bi, (d) C/C-SnO₂/Bi and (f) SnO₂.

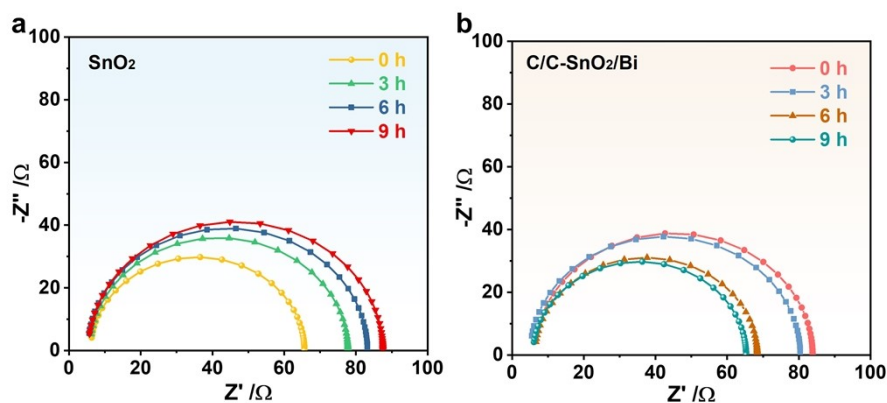


Fig. S6. Nyquist plots of (a) SnO_2 and (b) $\text{C/C-SnO}_2/\text{Bi}$ at 0, 3, 6, and 9 h under the durability test.

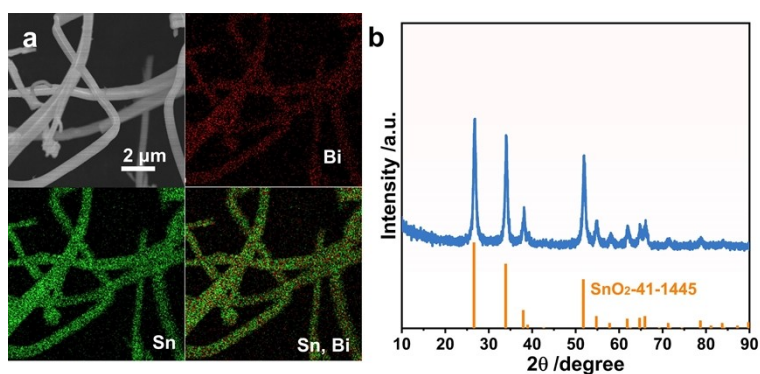


Fig. S7. (a) SEM-EDS elemental mappings and (b) PXRD pattern of $\text{C/A-SnO}_2/\text{Bi}$ after the durability test.

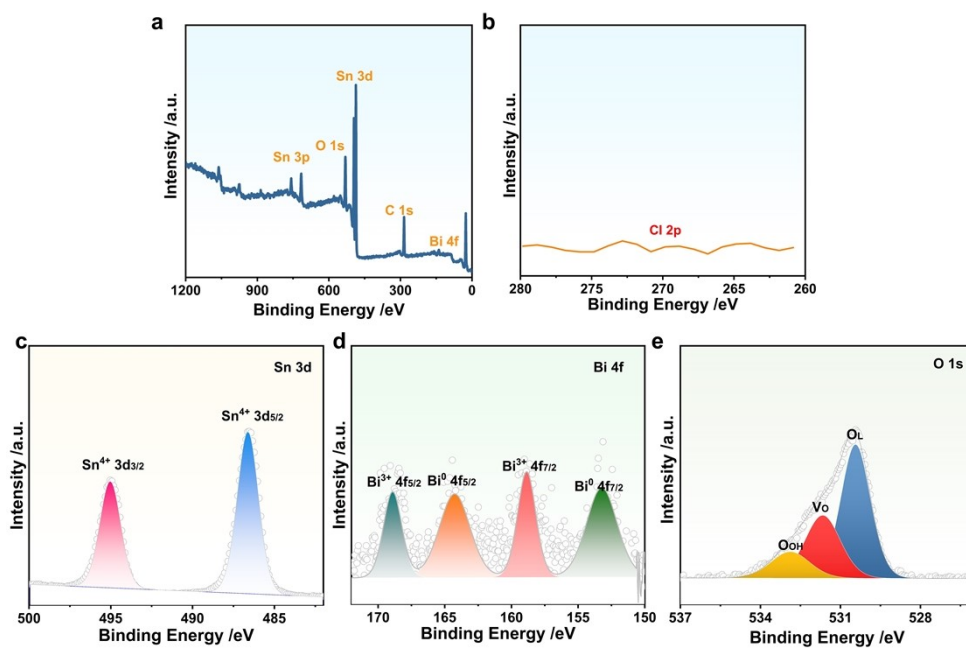


Fig. S8. (a) XPS survey spectrum, (b) the magnification of Cl 2p peak, (c) Sn 3d, (d) Bi 4f and (e) O 1s for $\text{C/A-SnO}_2/\text{Bi}$ after the durability test.

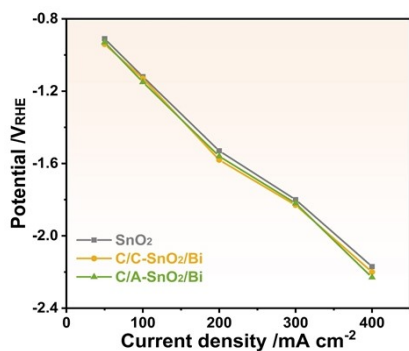


Fig. S9. The corresponding potentials of C/A-SnO₂/Bi, C/C-SnO₂/Bi and SnO₂ at different current densities in flow-cell.

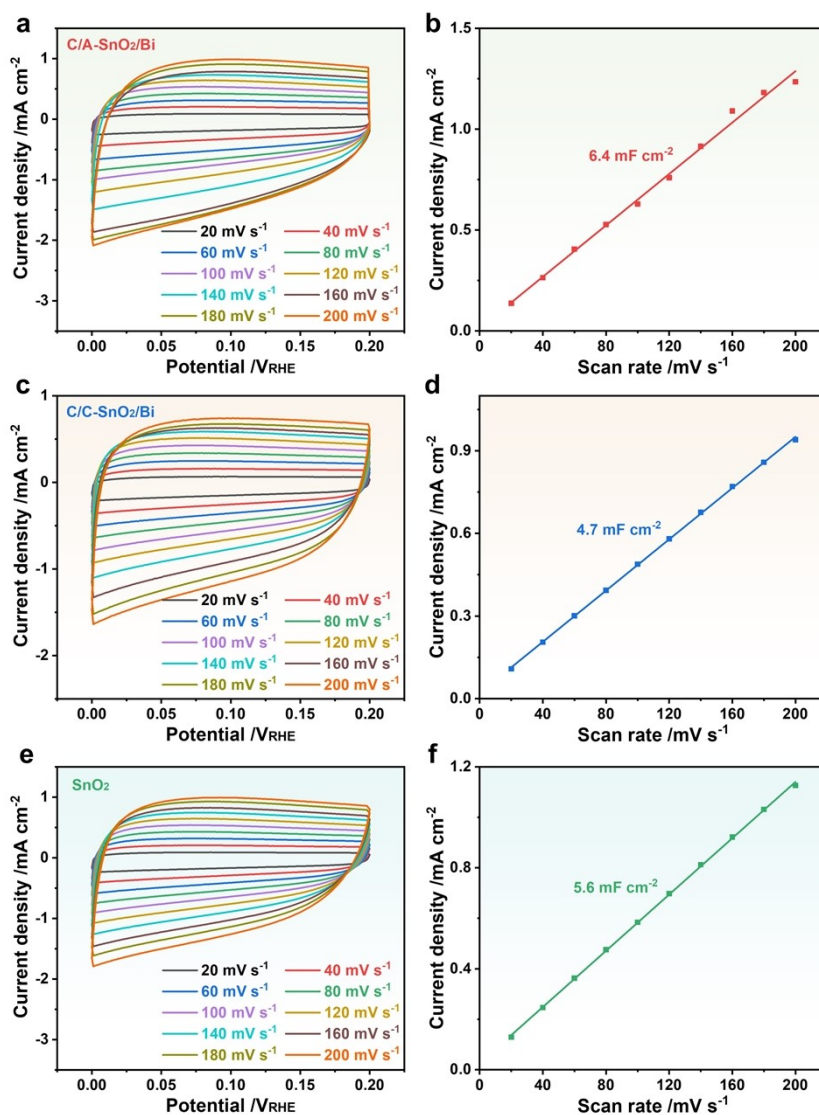


Fig. S10. CV curves of (a) C/A-SnO₂/Bi, (c) C/C-SnO₂/Bi and (e) SnO₂ with various scan rates. Charging current density differences plotted against scan rates for (b) C/A-SnO₂/Bi, (d) C/C-SnO₂/Bi and (f) SnO₂.

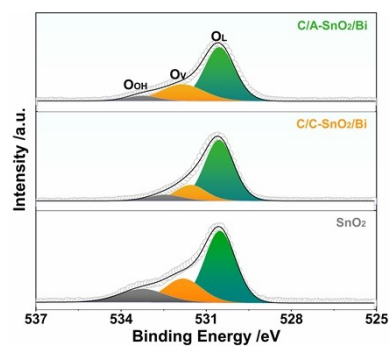


Fig. S11. O 1s spectra for C/A-SnO₂/Bi, C/C-SnO₂/Bi and SnO₂.

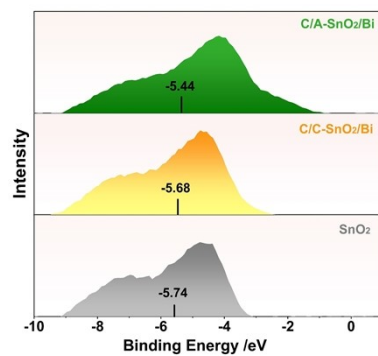


Fig. S12. Surface valence band spectra for C/A-SnO₂/Bi, C/C-SnO₂/Bi and SnO₂.

Table S1. ICP-MS results of the C/A-SnO₂/BiOCl.

Sample	Composition /%		
	Sn	Bi	Cl
C/A-SnO ₂ /BiOCl	85.6	8.2	6.2
C/A-SnO ₂ /Bi	91.5	8.5	/
C/C-SnO ₂ /Bi	90.2	9.8	/

Table S2. Comparison of CO₂RR performance on C/A-SnO₂/Bi NBs and another reported Sn or Bi-based catalysts.

Catalysts	H-cell Max. FE _{HCOOH} /%	Potential /V _{RHE}	Flow-cell Max. FE _{HCOOH} /%	Current density /mA cm ⁻²	Reference
C/A-SnO ₂ /Bi NBs	96.2	-1.3	81.2	400	This work
Bi ₁₉ Br ₃ S ₂₇	98	-1.1	90	150	[6]
Bi-S ₂	96.7	-0.9	97.8	150	[7]
Bi-Sn	93.9	-1.0	/	/	[8]
Bismuthene nanosheets	/	/	97.4	105.4	[9]
Cu-BiOC	/	/	99.8	800	[10]
SnO ₂ /LaOCl	90.1	-1.2	83.4	400	[11]
Bi ₂ O ₃ -FDCA-P	96.7	-1.2	93.60	120	[12]
BiOI	~98.4	-1.0	/	/	[13]
Bi-Sn/CF	96	-1.1	/	/	[14]
Sn _{0.80} Bi _{0.20}	/	/	95.8	74.6	[15]

Table S3. The proportion of lattice oxygen (O_L), oxygen vacancy (V_O) and surface hydroxyl/water (O_{OH}) of C/A-SnO₂/Bi, C/C-SnO₂/Bi and SnO₂.

Catalysts	O 1s		
	O _L /%	V _O /%	O _{OH} /%
C/A-SnO ₂ /Bi	54.88	36.59	8.53
C/C-SnO ₂ /Bi	70.40	18.77	10.83

References:

- [1] S. J. Clark, M. D. Segall, C. J. Pickard, P. J. Hasnip, M. I. J. Probert, K. Refson, M. C. Payne, Z. *Krist. Cryst. Mater.* **2005**, *220*, 567-570.
- [2] D. Vanderbilt, *Phys. Rev. B* **1990**, *41*, 7892-7895.
- [3] J. P. Perdew, K. Burke, M. Ernzerhof, *Phys. Rev. Lett.* **1996**, *77*, 3865-3868.
- [4] S. Grimme, *J. Comput. Chem.* **2006**, *27*, 1787-1799.
- [5] H. J. Monkhorst, J. D. Pack, *Phys. Rev. B* **1976**, *13*, 5188-5192.
- [6] X. Ma, Q. Wang, M. Wang, X. Jin, L. Wang, L. Zhang, *Chem. Eng. J.* **2023**, *474*, 145711.
- [7] M. Wang, S. Liu, B. Chen, M. Huang, C. Peng, *Chem. Eng. J.* **2023**, *451*, 139056.
- [8] Z. Wu, H. Wu, W. Cai, Z. Wen, B. Jia, L. Wang, W. Jin, T. Ma, *Angew. Chem. Int. Ed.* **2021**, *60*, 12554-12559.
- [9] W. Ma, J. Bu, Z. Liu, C. Yan, Y. Yao, N. Chang, H. Zhang, T. Wang, J. Zhang, *Adv. Funct. Mater.* **2021**, *31*, 2006704.
- [10] J. Lu, Y. Ren, J. Liang, L. Zou, Y. Gao, F. Li, J. Gao, J. Liu, *Small* **2024**, *20*, 2402879.
- [11] H. Li, H. Huang, W. Huang, X. Zhang, G. Hai, F. Lai, T. Zhu, S. Bai, N. Zhang, T. Liu, *Small* **2024**, *20*, 2402654.
- [12] Z. Han, Y. Chang, J. Gao, T. Liu, J. Li, J. Liu, J. Liu, Y. Gao, J. Gao, *Small* **2024**, *20*, 2403778.
- [13] J. Ma, J. Yan, J. Xu, J. Ni, H. Zhang, L. Lu, *Chem. Eng. J.* **2023**, *455*, 140926.
- [14] G. Wen, D.U. Lee, B. Ren, F.M. Hassan, G. Jiang, Z.P. Cano, J. Gostick, E. Croiset, Z. Bai, L. Yang, Z. Chen, *Adv. Energy Mater.* **2018**, *8*, 1802427.
- [15] Q. Yang, Q. Wu, Y. Liu, S. Luo, X. Wu, X. Zhao, H. Zou, B. Long, W. Chen, Y. Liao, L. Li, P.K. Shen, L. Duan, Z. Quan, *Adv. Mater.* **2020**, *32*, 2002822.